Grain size and phonon thermal conductivity of sintered bulk undoped lead telluride compacts processed via mechanical grinding and alloying

M. Bumrungpon[a], T. Maeda[b], M. Tachii[b], J. Asai[b], I. Morioka[b], R. Yasufuku[b], T. Hirai[b], T. Tsubochi[b], T. Kanaya[b], A. Dauscher[c] and K. Hasezaki[d]

[a]*Graduate School of Advanced Technology and Sciences, Tokushima University, 2-1 Minamijosanjima, Tokushima 770-8506, Japan*

[b]*Department of Mechanical Science, Division of Science and Technology, Graduate School of Sciences and Technology for Innovation, Tokushima University, 2-1 Minamijosanjima, Tokushima 770-8506, Japan*

[c]*Institut Jean Lamour, UMR 7198 CNRS-Université de Lorraine, 2 allée André Guinier-Campus ARTEM, BP 50840, 54011 Nancy Cedex, France*

[d]*Department of Mechanical Science, Graduate School of Technology, Industrial and Social Sciences, Tokushima University, 2-1 Minamijosanjima, Tokushima 770-8506, Japan*

**Corresponding author: hasezaki@tokushima-u.ac.jp*

Keywords: Thermoelectric materials, Chalcogenides, Electrical properties, Thermal conductivity

This study focused on investigating the influence of processing undoped, dense lead telluride (PbTe) either via mechanical grinding (MG) or mechanical alloying (MA), based on the milling rotation speed (1.5–3.0 Hz), followed by hot pressing (HP) on the grain size and phonon thermal conductivity (κ_{phonon}). The samples prepared via MG-HP were single-phased, had high relative densities (> 99%), and exhibited uniform morphologies. For a milling rate of 2.5 Hz, the minimum κ_{phonon} of MG-HP was 0.90 W m^{-1} K^{-1} and the average grain size was 0.47 μm. Furthermore, the grains produced by MG-HP and milled at 2.5 Hz comprised subgrains with a size of approximately 50 nm. The samples prepared using MA-HP showed higher theoretical relative densities. For a milling rate of 2.0 Hz, the minimum κ_{phonon} of MA-HP was 1.36 W m^{-1} K^{-1} and the average grain size was 0.52 μm. The electrical conductivity and Seebeck coefficient of MG-HP and MA-HP were similar to those of the *p*-type doped materials. Thus, the MG-HP process is an appropriate method for producing undoped PbTe with a high Seebeck coefficient and a low κ_{phonon}.

1. Introduction

Thermoelectric materials can transform thermal energy into electrical energy, and vice versa, thereby allowing waste heat to be harvested as useful electrical energy [1]. Several thermoelectric materials have been considered for power generation applications, such as GeTe [2], PbTe [3], half-Heuslers [4], Bi_2Te_3 [5], and silicides [6]. With no moving parts [7], thermoelectric generators provide long-duration operational reliability [8, 9]. The energy conversion in such materials can be determined using the dimensionless thermoelectric figure of merit (*ZT*), which is defined as

$$ZT = \alpha^2 \sigma \kappa^{-1} T \quad (1)$$

where α, σ, κ, and T denote the Seebeck coefficient (V K^{-1}), electrical conductivity (S m^{-1}), thermal conductivity (W m^{-1} K^{-1}), and absolute temperature (K), respectively.

The thermal conductivity mainly contributes to the phonon transport, κ_{phonon}, the carrier contribution from electron/hole transport, κ_{carrier}, and the bipolar transport, κ_{bipolar}.

$$\kappa = \kappa_{\text{phonon}} + \kappa_{\text{carrier}} + \kappa_{\text{bipolar}} = \kappa_{\text{phonon}} + L\sigma T + \frac{\sigma_h \sigma_e}{\sigma_h + \sigma_e}(\alpha_e - \alpha_h)^2 T \quad (2)$$

The carrier thermal conductivity, κ_{carrier}, is given by the Wiedemann–Franz law, where *L* denotes the Lorentz number [10, 11]:

$$L = (\pi k_B)^2 (3e^2)^{-1} = 2.45 \times 10^{-8}\ \text{W S}^{-1}\text{K}^{-2} \quad (3)$$

The bipolar thermal conductivity, κ_{bipolar}, is given by the electrical conductivities, σ_e and σ_h, and Seebeck coefficients, α_e and α_h of electron/hole transport [12, 13]. Increasing thermoelectric efficiency requires materials with high *ZT* values at operating temperatures [14]. Most optimizing strategies involve band structure engineering of the power factor ($\alpha^2\sigma$) or minimizing phonon-mediated heat transport. The reduction of thermal conductivity has attracted significant attention to improving *ZT* in thermoelectric materials. However, there have been studies indicating the importance of improving power factors in nanostructured thermoelectric materials [15, 16]. Recent attempts to improve thermoelectric materials focus on reducing the thermal conductivity [17, 18]. Finding the proper processing technique to reduce κ without reducing the electrical properties is still a challenge and requires further studies [19]. The main processes used to obtain fine grain thermoelectric materials for reducing the thermal conductivity are elements milling, mechanical alloying (MA), and alloyed ingot milling termed mechanical milling or grinding (MG). Repeated mechanical impact during planetary ball milling followed by hot pressing (HP) is a powerful method for preparing

homogeneous compounds that enables the formation of alloys in solid-state and has been previously used for preparing thermoelectric materials [20].

Doped PbTe is a promising thermoelectric material for applications in the intermediate temperature range of 500–900 K owing to its low κ_{phonon} and high α and σ [21]. PbTe (melting point 1197 K, theoretical density 8.26×10^{-3} kg m^{-3}) [22, 23] is a prime single-crystal thermoelectric material with low κ (~2 W m^{-1} K^{-1} at 300 K [24]) despite high symmetry. The material crystallizes within the NaCl structure (halite, cF8, space group Fm3m, No. 225), with Pb atoms occupying cationic sites and Te forming an anionic lattice. They are narrow bandgap semiconductors ($E_g \approx 0.25$ eV at 0 K, and 0.32 eV at 300 K) and exhibit either *n*-type or *p*-type conduction [25], depending on deviations from stoichiometry.

PbTe-based alloys are promising thermoelectric materials because of their high dependence on carrier concentration, low κ, and high-power factors. However, because of mechanical problems and particularly their subject to fracture, PbTe materials are difficult to process and have limited applications [26, 27]. To overcome mechanical and thermal stresses, reducing grain size is an effective hardening mechanism in PbTe [28]. In this study, the powder defines as an aggregate of particles. The particle consists of conjunctive grains, which consists of conjunctive subgrains. After sintering, the materials consist of conjunctive grains. Theoretical calculations of κ_{phonon} are related to grain size based on the Boltzmann equation and a heterostructure grain boundary model. The κ_{phonon} of undoped bulk PbTe at 400 K is constant from coarse grains to an average size of 1 μm and then sharply decreases for a grain size of 0.01 μm [29, 30]. Based on these theoretical calculations, the origin of the notable difference can be understood if one examines the grain size dependence of κ_{phonon}. The effects of grain boundaries for thermal conductivity are accounted for by a simple relaxation time formula, $T = L/ v_s$, where v_s and L denote the velocity of phonons and the grain size, respectively [29–31]. An improved theoretical analysis shows that the κ of PbTe with a grain size of 1 μm is approximately 5% lower than in similar materials with larger grain size, when compared with the single-crystal data [32].

High-energy ball milling is an efficient method to reduce the grain size [33, 34]. Subsequent sintering can produce grain growth but may partially repair the defects caused by milling. However, some of the studies show that obtained materials did not achieve a reduced κ_{phonon} less than 2 W m^{-1} K^{-1} at room temperature for large grain sizes [35, 36]. An earlier study reported on undoped PbTe prepared by mechanical alloying (MA) [37]. Differential scanning

calorimetry (DSC) indicated that MA was associated with an exothermic reaction heat between Pb and Te that promotes the rapid formation of PbTe and requires a milling time of 3 h for obtaining PbTe stoichiometric samples [38]. The sintered materials had a relative density of 76–79%. These studies indicated that strain should increase with milling time [39] because the material is placed under increasing stress, and that the crystallite size should decrease. Strain is representative of any defects (local disorder, dislocations, stacking faults). However, the crystallite size is significantly smaller than the grain size. A recent study established that lattice softening induced the internal strain by ball milling [40]. An increase in internal strain corresponds with a linear decrease in the speed of sound. In a previous study, the undoped PbTe prepared by alloyed ingot milling (MG) obtained a minimum κ_{phonon} of 1.29 W m^{-1} K^{-1} at room temperature [41].

Polycrystalline PbTe materials are generally synthesized in an evacuated and sealed quartz tube heated to the melting temperature of the material. This conventional synthesis is restricted for industrial applications because the process is long and requires high temperatures to prevent segregation. Mechanical alloy processing and hot pressing (MA-HP) produce thermoelectric materials without melting [42]. High-energy milling activates local reactions among elements when the raw materials are sufficiently refined and in close proximity. MA produces high exothermic heat as Pb and Te react, and the grain boundary scattering produces a refining effect. To maintain a low κ_{phonon}, fine-grained material is normally prepared using mill processes such as MG and MA. MG and MA followed by HP can synthesize materials with uniform element distribution.

A direct comparison between undoped PbTe prepared by MG and MA could provide additional information regarding the precise impact of the MG and MA processes on the microstructures and electrical properties, which are not directly accessible, as compared to conventional melt-growth alloys [43]. The reduction of κ_{phonon} is related to the grain size. The FIB-SEM images for the sintered grain size were investigated.

2. Material and Methods

The MG-HP samples of PbTe were prepared by melting and dry-ball milling, followed by HP. The initial PbTe ingots produced for further MG were synthesized from high-purity Pb (99.998%, 3–5 mm grain size) and high-purity Te (99.9999%, 2 mm grain size) from the Koujundo Chemical Laboratory Co., Ltd. Stoichiometric amounts of these elements for the targeted PbTe compositions were placed in clean carbon-coated ampoules with a columnar-cone-shaped bottom (10 mm inner diameter, 120 mm length). The ampoules were sealed under 0.1 Pa and heated to 1123 K in a furnace for 5 h. The material enclosed in the ampoule was quenched in a room temperature water bath. The ampoules were then broken, the alloyed PbTe ingot was removed, and the ingot was transferred to the milling vessel. The directly milled ingot was approximately 10 mm in diameter and 20 mm long. MG of the ingots and MA from the raw Pb and Te were performed in yttria-stabilized zirconia (YSZ) ceramic vessels (2.5×10^{-4} m^{-3} capacity) and balls (25 mm diameter). The weight ratio of the milling balls to the ingots or raw materials was 20:1. The milling was performed using a Fritsch P-5 planetary ball mill. The vessels and balls were sealed in a glove box under Ar atmosphere to prevent oxidation of the powder during milling. Milling was performed at 1.5–3.0 Hz for 30 h. In an Ar-filled glove box, the milled or alloyed powder was passed through a polymer mesh sieve (150 μm diameter). The sieved powder was placed in an HP mold and compacted under an Ar atmosphere at 650 K under a uniaxial pressure of 196 MPa. The samples were prepared under an Ar atmosphere, except when the HP mold was exposed to air during the transfer between the glove box and HP chamber. The sintered ingots (8–10 mm thick, 10 mm diameter) were cut into disks (1 mm thick, 10 mm diameter) to determine the Seebeck coefficient and the electrical and thermal conductivities. The density was determined using the Archimedes method at room temperature, with absolute and relative density accuracies better than ±0.2%.

The PbTe phase homogeneity and microstructures were investigated by X-ray diffraction (XRD; Rigaku SmartLab, Cu Kα radiation), scanning electron microscopy (SEM; JEOL, JSM-6510A), and focused ion beam (FIB; JEOL, JEM-9320). XRD patterns in the out-of-plane directions of the PbTe sintered disks on the glass plate were recorded in the Bragg angle range of $2\theta = 20–90^{\circ}$. General scans with a step size of 0.1° and step time of 0.5 s were conducted for phase identification.

The microstructures and grain sizes of the cross sections were examined using FIB-SEM and energy-dispersive X-ray spectroscopy (EDS). The surfaces of the sintered PbTe disks were then polished and chemically etched. Agglomerate-free alumina powder and alumina suspensions

were used as the polishing grits. The average grain sizes were observed using FIB-SEM and measured via the linear intercept technique for two-phase polycrystalline, as follows [44]:

$$\overline{D} = 1.56\ \frac{C}{MN} \quad (4)$$

where $\overline{D}$ denotes the average grain size, C the total length of the test line used, N the number of intercepts, and M the photomicrograph magnification. The proportionality constant (1.56), is a correction factor derived by Mendelson for random slices using a model system consisting of space-filling tetrahedrally shaped gains with a long normal size distribution. The elemental dispersion profiles of the PbTe cross sections were determined using EDS.

Electrical conductivity was measured using a four-point probe (1.0 mm probe, tungsten carbide) with a delta-mode electrical resistance system, based on a 2182A/6220 instrument (Keithley Instruments, Inc.). The electrical conductivity was confirmed based on ohmic contact to have an accuracy better than ±1%. The Seebeck coefficient was determined using the constructed thermal contact method [45]. A standard BiTe thermoelectric material (SRM 3451) was used as the reference sample to confirm that the accuracy was better than ±2% at room temperature. The thermal conductivity was measured at room temperature under 1 Pa vacuum using a static comparison method [46]. Quartz (κ = 1.411 W m^{-1} K^{-1}) was used as a reference sample, and the accuracy was better than ±1% when using the same quartz disk for both the measurement and reference positions. The PbTe sample and quartz were inserted between copper blocks 10 mm in diameter for a static comparison of the thermal conductivity.

3. Results and discussion

XRD analysis of the processed MG powder showed that only the PbTe phase was obtained, with the absence of any secondary phase. After HP, all PbTe samples prepared by either MG-HP or MA-HP were dense and *p*-type semiconductors. Table 1 shows that the absolute and relative densities of the MG-HP and MA-HP samples depended on the milling rotation speed. Samples prepared by the MG-HP process had relative densities close to 99%, which is higher than the results reported by Bouad et al. [37]. The MA-HP samples exhibited densities significantly higher than the theoretical bulk density. This may be because of the increased interior temperature in the milling vessels during the process owing to the high exothermic reaction heat between Pb and Te [38]. The vapor pressures of PbTe, Pb, and Te are less than 10^{-6}, 10^{-5}, and 1 Pa at 650 K, respectively [47, 48]. Because Te has a higher vapor pressure than PbTe and Pb, Te evaporates during the milling process [23], leading to excess Pb and higher densities.

Table 1 Milling rotation speed and densities of MG–HP and MA–HP PbTe samples.

Rotation speed (Hz)	Absolute density ρ/ 10^{-3} kg m^{-3}, relative density (%)	
	MG-HP	MA-HP
1.50	8.23, 99.7	8.33, 100.9
1.83	8.23, 99.7	8.30, 100.5
2.00	8.20, 99.3	8.30, 100.5
2.33	8.21, 99.4	8.36, 101.3
2.50	8.21, 99.4	8.40, 101.7
2.67	8.22, 99.6	8.38, 101.5
3.00	8.24, 99.9	8.39, 101.5

Theoretical density 8.26×10^{-3} kg m^{-3} [23].

Figure 1(a) shows a SEM image of a cross section of the MG-HP sample milled at 2.5 Hz. This sample exhibited a dense and uniform morphology. These results indicate that contamination by the erosion of the milling vessel and balls and the rotation speed did not affect the texture. Figure 1(b) shows a SEM image obtained at high magnification. The dark particle with a diameter of approximately 2 μm is a contaminated particle from the milling vessel and balls. These particles correspond to YSZ, and they did not react with PbTe because a reaction layer

between the YSZ and PbTe matrix was not observed (see Supplementary data A).

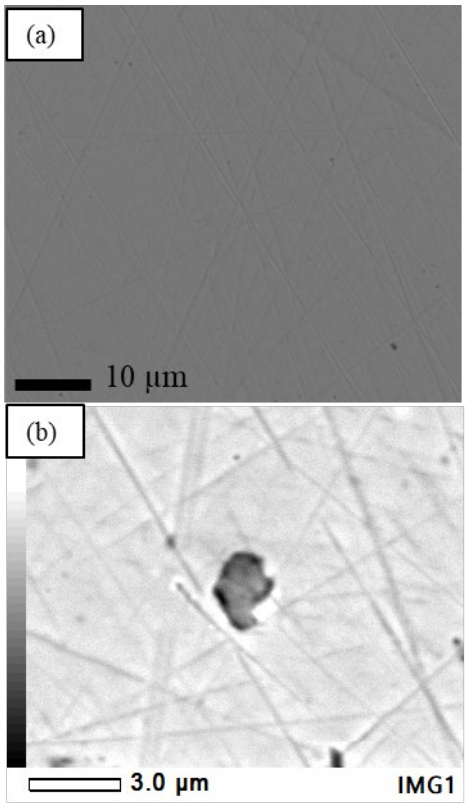

Fig. 1 SEM images of a cross-section of the PbTe sample milled at 2.5 Hz prepared by MG-HP.

Figures 2(a)–(c) and 2(d)–(f) show FIB-SEM images of MG-HP and MA-HP PbTe milled at 1.5, 2.5, and 3.0 Hz, respectively. The PbTe samples consisted of dense and fine grains. The linear intercept technique [44] was applied to calculate the average grain size of the PbTe samples prepared using MG-HP and MA-HP (Figure 3). At 1.5–2.0 Hz the average grain size decreases, and at 2.0–3.0 Hz it tends to stabilize when the rotation speed is increased. The smallest average grain size, 0.47 µm, was obtained for the PbTe sample produced by MG-HP and milled at 2.5 Hz. The grains consisted of subgrains approximately 50 nm in size, based on the TEM observations (see Supplementary data B). For the PbTe samples produced by MA-HP, the smallest average grain size is 0.52 µm, alloyed at 2.0 Hz. The average grain size is slightly higher for MA-HP than for MG-HP samples processed at 2.33–3.0 Hz owing to the exothermic reactions during the MA process [38]. The MG process induces kinetic energy, whereas the MA process induces kinetic energy and a high exothermic reaction heat [38].

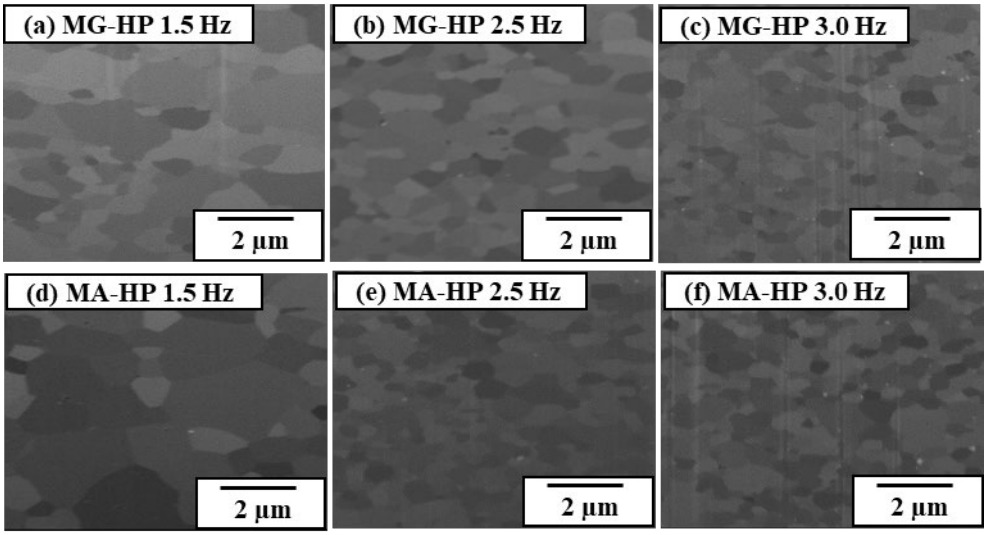

Fig. 2 FIB-SEM micrographs of PbTe samples prepared by MG-HP from (a)-(c) and MA-HP from (d)-(f) at 1.5, 2.5 and 3.0 Hz.

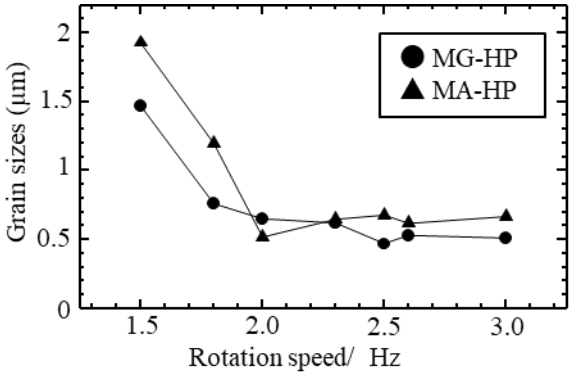

Fig. 3 Grain sizes (μm) and milling rotation speed related to PbTe samples prepared by MG-HP and MA-HP.

Figure 4 shows a sequence of XRD patterns obtained at 2θ = 20–90º for PbTe MG-HP and MA-HP samples milled at rotation speeds of 1.5–3.0 Hz. All the peaks from MG-HP could be indexed to the PbTe structure, and no other peaks were observed. Additionally, Figure 5 shows the enhanced intensity scale shown in Figure 4. In the absence of YSZ, Pb peaks occur at 31.327 and 36.332° for the MA-HP sample processed at 3.0 Hz. This analysis explains the density enhancement in the MA-HP cases, which is consistent with the differential thermal analysis (DTA) results (see Supplementary data C).

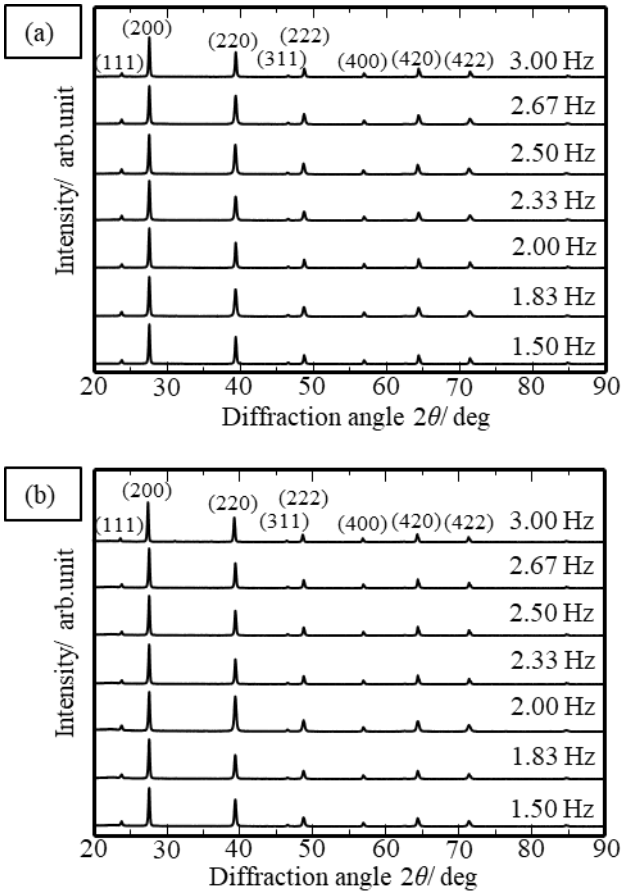

Fig. 4 XRD patterns of PbTe MG-HP (a) and MA-HP (b) samples milled at rotation speed from 1.5 to 3.0 Hz, and PbTe main indexes [23].

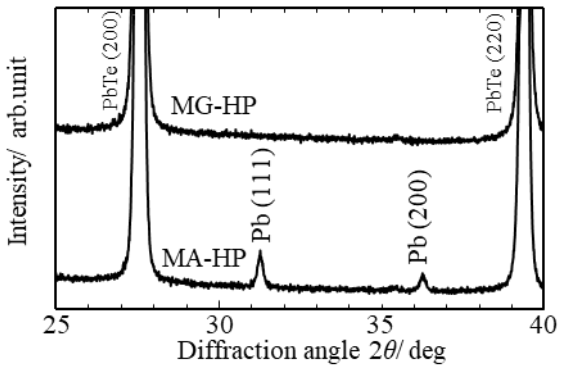

Fig. 5 XRD patterns of PbTe MG-HP and MA-HP samples milled at 3.0 Hz. Enhancement of the intensity scale from 25° to 40° 2θ range, Pb peaks appear at 31.327° and 36.332° for the MA-HP sample milled at 3.0 Hz.

Figure 6 shows the variations of the Seebeck coefficient, α, at room temperature based on the milling rotation speed for the PbTe samples prepared by MG-HP or MA-HP. For the MG-HP samples, the Seebeck coefficient decreased as the rotational speed increased. The maximum value, 494 μV K^{-1}, was obtained for the MG-HP sample milled at 1.5 Hz. The Seebeck coefficient of the MG-HP samples slightly decreased at high rotation speeds and was higher than that of samples prepared by MA-HP. The Te vacancies act as dopants and reduce the Seebeck coefficient. The MG-HP process prevents Te evaporation so that the MG-HP samples exhibit near PbTe stoichiometry and thus a higher Seebeck coefficient. The Seebeck coefficient of the MG-HP samples decreased with increasing rotation milling speed, particularly at 2.5–3.0 Hz. For MA-HP samples, because Te deficiency acts as a dopant, the Seebeck coefficient behaves like *p*-type doped materials.

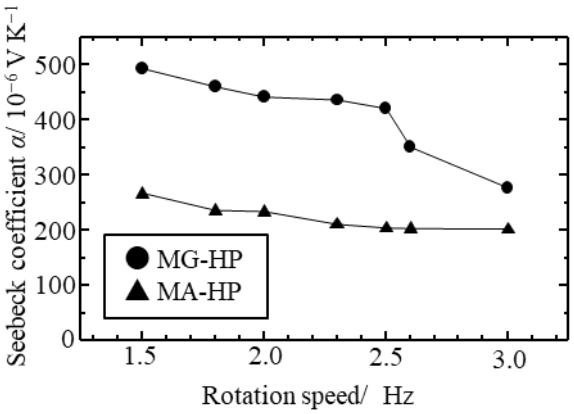

Fig. 6 Seebeck coefficient α at room temperature and milling rotation speed related to PbTe samples prepared by MG-HP and MA-HP.

Figure 7 shows the electrical conductivity, σ, at room temperature as a function of the milling rotation speed for the PbTe samples prepared by MG-HP and MA-HP. The electrical conductivity of the MG-HP and MA-HP samples increased with milling rotation speed. The electrical conductivity of MG-HP is lower than that of MA-HP. The loss of Te induced by the process, as described previously, led to a Te deficiency in PbTe at high rotation speeds, and thus it is vital that the process is energetic. Thus, the electrical conductivities of the PbTe samples produced by MA-HP were higher than those of the MG-HP processed samples. The large number of Te deficiencies created during milling led to an increase in electrical conductivity. However, Te deficiency may be at the limit of the PbTe solid solution, as shown in Figure 5. The effect of Te deficiency is consistent with the results showing that the MA-HP samples have a relative density above the theoretical density, as shown in Table 1. For MA-HP

samples, because Te deficiency acts as a dopant, the electrical conductivity and Seebeck coefficient behave like *p*-type doped materials. The inverse relationship between the electrical conductivity and Seebeck coefficient is consistent with the dependence of the electrical conductivity and Seebeck coefficient on the concentration of free carriers [20].

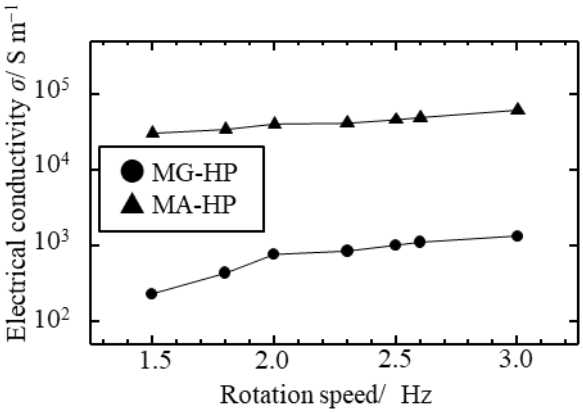

Fig. 7 Electrical conductivity σ at room temperature and milling rotation speed related to PbTe samples prepared by MG-HP and MA-HP.

Figure 8 shows the total thermal conductivity, κ_{total}, and phonon thermal conductivity, κ_{phonon}, at room temperature as a function of the milling rotation speed for the PbTe samples prepared by MG-HP or MA-HP. The κ_{phonon} values were estimated from Equations (2) and (3) and show that κ_{phonon} behavior depends on the preparation process. The minimum κ_{phonon} of the MG-HP sample was 0.90 W m^{-1} K^{-1} obtained after milling at 2.5 Hz with an average grain size of 0.47 μm. The minimum κ_{phonon} of the MA-HP samples was 1.36 W m^{-1} K^{-1} for the sample milled at 2.0 Hz, exhibiting an average grain size of 0.52 μm.

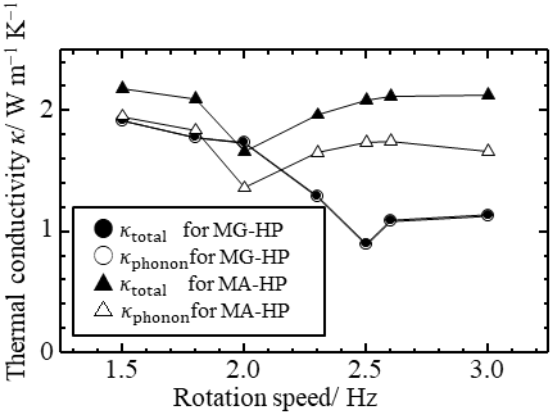

Fig. 8 Total thermal conductivity κ_{total} and phonon thermal conductivity κ_{phonon} at room temperature and milling rotation speed related to PbTe samples prepared by MG-HP and MA-HP.

The κ_{phonon} for the PbTe samples prepared by MG-HP and MA-HP at a rotation speed of 1.5 Hz are near identical. Grains with an average size of over 1 μm (1.47–1.93 μm) can be clarified using theoretical calculations [29, 30] based on the grain boundary scattering caused by coarse grain sizes and lead to high κ_{phonon} values. The κ_{phonon} of MG-HP samples tends to decrease with an increase in the rotation speed because of the decreased grain sizes (including fine grains). However, the samples produced by MA-HP also exhibited decreased κ_{phonon} values with increasing milling rotation speeds up to 2.0 Hz, which then increased and stabilized from 2.0–3.0 Hz because of the high milling energy and exothermic reaction heat. Furthermore, κ_{phonon} slightly increases with the grain growth.

In addition, theoretical calculations by Yoshino [29, 30] based on the grain boundary scattering mechanism indicates that at 400 K, the κ_{phonon} of undoped PbTe with an average grain size above 1 μm is constant, but sharply decreases at a grain size of approximately 0.01 μm. The grain size is critical for κ_{phonon} transition. Figure 9 shows that the trend of κ_{phonon} at room temperature depends on grain size for samples prepared by MG-HP and MA-HP. This trend is similar to what was obtained from theoretical calculations. However, κ_{phonon} changes significantly at approximately 1 μm. The value is different from theoretical calculations based on the grain boundary scattering mechanism [29, 30]. The grains consisted of subgrains approximately 50 nm in size produced by MG-HP milled at 2.5 Hz from the TEM observations (see Supplementary data B). Considering the size of the subgrain, the relationship of the phonon thermal conductivity and grain size including the subgrain corresponds with the theoretical calculation.

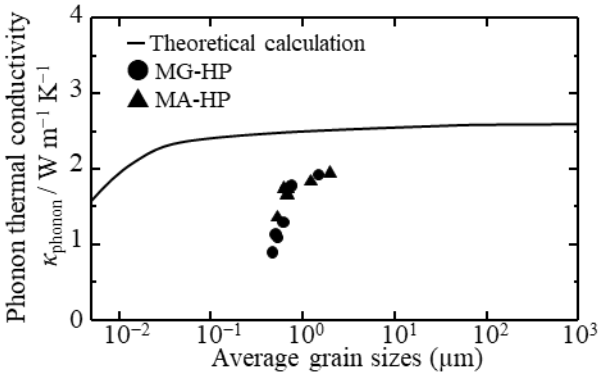

Fig. 9 Phonon thermal conductivity κ_{phonon} at room temperature and average size of PbTe samples prepared by MG-HP and MA-HP compared with theoretical calculation at 400 K [29, 30].

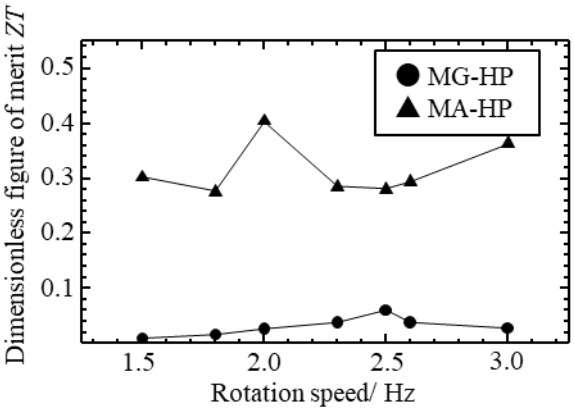

Fig. 10 Dimensionless figure of merit *ZT* at room temperature and milling rotation speed related to PbTe samples prepared by MG-HP and MA-HP.

Figure 10 shows the dimensionless figure of merit, *ZT*, at room temperature as a function of the milling rotation speed for the PbTe samples prepared using MG-HP and MA-HP. The MA-HP sample milled at 2.0 Hz had a maximum *ZT* of 0.41 (α: 234 μV K^{-1}; σ: 4.12 × 10^4 S m^{-1}; κ: 1.66 W m^{-1} K^{-1}) at room temperature.

It should be noted that MG-HP produces near stoichiometric finer grains, and lower κ_{phonon} values than MA-HP. Undoped PbTe samples produced by MG-HP had fine grains and high microstrains, with high Seebeck coefficients and a low κ_{phonon}. The samples prepared by MA-HP behaved like *p*-type doped materials owing to the Te deficiency. These results further demonstrate that the melting process in MG-HP is necessary for the preparation of these specific experimental conditions.

4. Conclusions

In this study, the thermoelectric properties of undoped PbTe prepared by MG and MA processes at various rotation speeds, followed by HP, were investigated. The results are summarized as follows:

1. The samples prepared using MG-HP were obtained as a single phase. The samples prepared using MG-HP had a high relative density of approximately 99%. The density of the samples prepared using MA-HP was above the theoretical value because of the remaining Pb. During the MA process, the high exothermic reaction heat between Pb and Te caused Te evaporation because Te has a higher vapor pressure than Pb.
2. For the samples prepared by MG-HP, at 2.5 Hz, the minimum κ_{phonon} was 0.90 W m^{-1} K^{-1} and the average grain size was 0.47 μm. The grains consisted of subgrains with a size of approximately 50 nm produced by MG-HP and milled at 2.5 Hz. For the samples prepared by MA-HP, at 2.0 Hz, the minimum κ_{phonon} is 1.36 W m^{-1} K^{-1} and the average grain size is 0.52 μm. MG-HP produced finer grains and a lower κ_{phonon} than MA-HP. The MG process produces kinetic energy, whereas the MA process produces kinetic energy and highly exothermic reaction heat. This led to the differences in the grain size.
3. The κ_{phonon} of grain sizes over 1 μm agreed with theoretical calculations of the grain boundary scattering mechanism.
4. Because Te deficiency acts as a dopant, the electrical conductivity and Seebeck coefficient in the MG-HP and MA-HP samples behave in a similar manner to *p*-type doped materials.
The MG-HP process is an appropriate method for producing undoped PbTe with high Seebeck coefficient, low κ_{phonon}, and high-density thermoelectric materials. It is applicable not only to PbTe, but also to other thermoelectric materials.

Authors statement

M. Bumrungpon: Conceptualization, methodology, investigation, writing – original draft, writing – review, and editing.

T. Maeda: Methodology, investigation of electrical properties and microstructural characterization.

M. Tachii: Raw materials preparation, investigation of thermal conductivity.

J. Asai: Methodology, investigation of DTA results.

I. Morioka: Investigation of FIB-SEM results.

R. Yasufuku: Investigation of XRD results.

T. Hirai: Investigation of XRD results.

T. Tsubochi: Investigation of SEM and XRD results.

T. Kanaya: Formal analysis of thermoelectric properties.

A. Dauscher: Conceptualization, writing – review and editing.

K. Hasezaki: Conceptualization, methodology, writing – review and editing, supervision, and project administration.

Declaration of competing interest

The authors declare that they have no known competing financial interests or personal relationships that could have influenced the research reported in this study.

Acknowledgments

The authors express our thanks to Emeritus Prof. Yasutoshi Noda (Shimane University, Japan) for valuable discussions on the preparation of PbTe-based ingots. We thank “Elsevier's English Language Editing Service” and Assoc. Prof. Don Sturge (Tokushima University) for editing the English text of a draft of this manuscript. This study was supported by the Takahashi Industrial and Economic Research Foundation.

Data availability

The processed data required to reproduce these findings are available for download from the supporting file (Supplementary data A, B, and C).

References

[1] D.M. Rowe, Thermoelectrics and its Energy Harvesting, CRC press, Taylor & Francis Group, Boca Raton, Florida, 2018, pp. 1-12.

[2] X. Zhang, Z. Bu, S. Lin, Z. Chen, W. Li, Y. Pei, GeTe Thermoelectrics, Joule, 4 (2020) 986-1003. https://doi.org/10.1016/j.joule.2020.03.004.

[3] P.K. Sharma, T.D. Senguttuvan, V.K. Sharma, S. Chaudhary, Revisiting the thermoelectric properties of lead telluride, Mater. Today Energy, 21 (2021) 100713. https://doi.org/10.1016/j.mtener.2021.100713.

[4] W. Ren, X. Shi, Z. Wang, Z. Ren, Crystallographic design for half-Heuslers with low lattice thermal conductivity, Mater. Today Phys., 25 (2022) 100704. https://doi.org/10.1016/j.mtphys.2022.100704**.**

[5] Y. Saberi, S.A. Sajjadi, A comprehensive review on the effects of doping process on the thermoelectric properties of Bi_2Te_3 based alloys, J. Alloys Compd., 904 (2022) 163918. https://doi.org/10.1016/j.jallcom.2022.163918.

[6] A. Nozariasbmarz, A. Agarwal, Z.A. Coutant, M.J. Hall, J. Liu, R. Liu, A. Malhotra, P. Norouzzadeh, M.C. Oeztuerk, V.P. Ramesh, Thermoelectric silicides: A review, Jpn. J. Appl. Phys., 56 (2017) 05DA04. https://doi.org/10.7567/JJAP.56.05DA04.

[7] H.J. Goldsmid, Introduction to thermoelectricity, Springer, New York, 2016, pp. 1-7. https://doi.org/10.1007/978-3-642-00716-3_1.

[8] Y. Shinohara, Recent progress of thermoelectric devices or modules in Japan, Mater. Today: Proc., 4 (2017) 12333-12342. http://doi.org/10.1016/j.matpr.2017.10.001.

[9] Y. Takagiwa, Y. Shinohara, A practical appraisal of thermoelectric materials for use in an autonomous power supply, Scripta Mater., 172 (2019) 98-104. https://doi.org/10.1016/j.scriptamat.2019.07.022.

[10] T.M. Tritt, Thermal conductivity: Theory, Properties, and Applications, Kluwer Academic/ Plenum Publishers, New York, 2004, pp. 1-17. https://doi.org/10.1007/b136496.

[11] C.H. Su, Experimental determination of lattice thermal conductivity and Lorenz number as functions of temperature for *n*-type PbTe, Mater. Today Phys., 5 (2018) 58-63. https://doi.org/10.1016/j.mtphys.2018.05.005.

[12] P.J. Price, Ambipolar thermodiffusion of electrons and holes in semiconductors, London, Edinburgh, Dublin Philos. Mag. J. Sci. 46 (1955) 1252–1260. https://doi.org/10.1080/14786441108520635.

[13] G.S. Nolas, J. Sharp, H.J. Goldsmid, Thermoelectrics Basic Principles and New Materials Developments, Springer, Berlin, Heidelberg, 2001, pp.42-44.
[14] J. Shuai, J. Mao, S. Song, Q. Zhang, G. Chen, Z. Ren, Recent progress and future challenges on thermoelectric Zintl materials, Mater. Today Phys., 1 (2017) 74-95. https://doi.org/10.1016/j.mtphys.2017.06.003.
[15] Devender, P. Gehring, A. Gaul, A. Hoyer, K. Vaklinova, R.J. Mehta, M. Burghard, T. Borca-Tasciuc, D.J. Singh, K. Kern, G. Ramanath, Harnessing Topological Band Effects in Bismuth Telluride Selenide for Large Enhancements in Thermoelectric Properties through Isovalent Doping, Adv. Mater., 28 (2016) 6436-6441. https://doi.org/10.1002/adma.201601256.
[16] J. Kennedy, P.P. Murmu, P. Kumar, G. Ramanath, Multifold enhancements in thermoelectric power factor in isovalent sulfur doped bismuth antimony telluride films, Mater. Res. Bull., 142 (2021) 111426. https://doi.org/10.1016/j.materresbull.2021.111426.
[17] K. Biswas, J. He, I.D. Blum, C.-I. Wu, T.P. Hogan, D.N. Seidman, V.P. Dravid, M.G. Kanatzidis, High-performance bulk thermoelectrics with all-scale hierarchical architectures, Nature, 489 (2012) 414-418. https://doi.org/10.1038/nature11439.
[18] K. Zhang, Q. Zhang, L. Wang, W. Jiang, L. Chen, Enhanced thermoelectric performance of Se-doped PbTe bulk materials via nanostructuring and multi-scale hierarchical architecture, J. Alloys Compd., 725 (2017) 563-572. https://doi.org/10.1016/j.jallcom.2017.07.193.
[19] J. He, T.M. Tritt, Advances in thermoelectric materials research: Looking back and moving forward, Science, 357 (2017) eaak9997. https://doi.org/10.1126/science.aak9997.
[20] D.M. Rowe, General principles and theoretical consideration, in: D.M. Rowe (Ed.), Thermoelectr. Handb. Macro to Nano, CRC Press, Taylor & Francis Group, Boca Raton, Florida, 2006, ch. 1 and 19.
[21] Y. Pei, X. Shi, A. LaLonde, H. Wang, L. Chen, G.J. Snyder, Convergence of electronic bands for high performance bulk thermoelectrics, Nature, 473 (2011) 66. https://doi.org/10.1038/nature09996.
[22] D.R. Lide, CRC handbook of chemistry and physics: A Ready-Reference Book of Chemical and Physical Data, CRC press, Taylor& Francis Group, Boca Raton, Florida, 1995, pp. 4-64. https://doi.org/10.1021/ja041017a.
[23] E. Rogacheva, I. Krivulkin, V. Popov, T. Lobkovskaya, Concentration dependences of properties in $Pb_{1-x}Mn_xTe$ solid solutions, Phys. stat. sol. (a), 148 (1995) K65-K67. https://doi.org/10.1002/pssa.2211480235.

[24] I. Ravich Yu, B. Efimova, I. Smirnov, Semiconducting lead chalcogenides, Plenum, New York, 1970, pp. 156-227.
[25] C. Chubilleau, B. Lenoir, A. Dauscher, C. Godart, Low temperature thermoelectric properties of PbTe–$CoSb_3$ composites, Intermetallics, 22 (2012) 47-54. https://doi.org/10.1016/j.intermet.2011.10.023.
[26] Y. Gelbstein, G. Gotesman, Y. Lishzinker, Z. Dashevsky, M.P. Dariel, Mechanical properties of PbTe-based thermoelectric semiconductors, Scripta Mater., 58 (2008) 251-254. https://doi.org/10.1016/j.scriptamat.2007.10.012.
[27] Y. Gelbstein, $Pb_{1-x}Sn_xTe$ Alloys: Application Considerations, J. Electron. Mater., 40 (2011) 533-536. https://doi.org/10.1007/s11664-010-1435-6.
[28] J.E. Ni, E.D. Case, K.N. Khabir, R.C. Stewart, C.-I. Wu, T.P. Hogan, E.J. Timm, S.N. Girard, M.G. Kanatzidis, Room temperature Young's modulus, shear modulus, Poisson's ratio and hardness of PbTe–PbS thermoelectric materials, Mater. Sci. Eng., B, 170 (2010) 58-66. https://doi.org/10.1016/j.mseb.2010.02.026.
[29] J. Yoshino, Theoretical estimation of thermoelectric figure of merit in sintered materials and proposal of grain-size-graded structures, Functionally Graded Materials 1996, (Elsevier, Amsterdam, 1997), pp. 495-500. https://doi.org/10.1016/B978-044482548-3/50081-0.
[30] J. Yoshino, Thermoelectric Energy Conversion, M. Sakata (Ed.) Theory and Application, Shokabo, Tokyo, 2005, pp. 44-51.
[31] J. Parrott, The thermal conductivity of sintered semiconductor alloys, J. phys., C, Solid State Phys., 2 (1969) 147. https://doi.org/10.1088/0022-3719/2/1/320.
[32] C. Bhandari, D. Rowe, High-temperature thermal transport in heavily doped small-grain-size lead telluride, Appl. Phys. A, 37 (1985) 175-178. https://doi.org/10.1007/BF00617503.
[33] S. Yoon, O.J. Kwon, S. Ahn, J.-Y. Kim, H. Koo, S.-H. Bae, J.-Y. Cho, J.-S. Kim, C. Park, The Effect of Grain Size and Density on the Thermoelectric Properties of Bi_2Te_3-PbTe Compounds, J. Electron. Mater., 42 (2013) 3390-3396. https://doi.org/10.1007/s11664-013-2753-2.
[34] C. Papageorgiou, E. Hatzikraniotis, C.B. Lioutas, N. Frangis, O. Valassiades, K.M. Paraskevopoulos, T. Kyratsi, Thermoelectric Properties of Nanocrystalline PbTe Synthesized by Mechanical Alloying, J. Electron. Mater., 39 (2010) 1665-1668. https://doi.org/10.1007/s11664-010-1234-0.
[35] M.H. Lee, J.H. Park, S.-D. Park, J.-S. Rhyee, M.-W. Oh, Grain growth mechanism and thermoelectric properties of hot press and spark plasma sintered Na-doped PbTe, J. Alloys Compd., 786 (2019) 515-522. https://doi.org/10.1016/j.jallcom.2019.01.387.

[36] A. Schmitz, C. Stiewe, K. Zabrocki, J. de Boor, K. Mull, E. Müller, Current assisted sintering of PbTe—Effects on thermoelectric and mechanical properties, Mater. Res. Bull., 86 (2017) 159-166. https://doi.org/10.1016/j.materresbull.2016.10.023.
[37] N. Bouad, R. Marin-Ayral, J. Tedenac, Mechanical alloying and sintering of lead telluride, J. Alloys Compd., 297 (2000) 312-318. https://doi.org/10.1016/S0925-8388(99)00611-8.
[38] N. Bouad, R.M. Marin-Ayral, G. Nabias, J.C. Tédenac, Phase transformation study of Pb–Te powders during mechanical alloying, J. Alloys Compd., 353 (2003) 184-188. https://doi.org/10.1016/s0925-8388(02)01179-9.
[39] N. Bouad, L. Chapon, R.M. Marin-Ayral, F. Bouree-Vigneron, J.C. Tedenac, Neutron powder diffraction study of strain and crystallite size in mechanically alloyed PbTe, J. Solid State Chem., 173 (2003) 189-195. https://doi.org/10.1016/s0022-4596(03)00017-3.
[40] R. Hanus, M.T. Agne, A.J. Rettie, Z. Chen, G. Tan, D.Y. Chung, M.G. Kanatzidis, Y. Pei, P.W. Voorhees, G.J. Snyder, Lattice Softening Significantly Reduces Thermal Conductivity and Leads to High Thermoelectric Efficiency, Adv. Mater., 31 (2019) 1900108. https://doi.org/10.1002/adma.201900108.
[41] M. Bumrungpon, I. Morioka, R. Yasufuku, T. Hirai, K. Hanasaku, K. Hirota, K. Takagi, K. Hasezaki, The Critical Point of Average Grain Size in Phonon Thermal Conductivity of Fine-Grained Undoped Lead Telluride, Mater. Trans., 61 (2020) 2025-2029. https://doi.org/10.2320/matertrans.MT-M2020069.
[42] O. Falkenbach, M.O. Loeh, C.W. Wiegand, A. Schmitz, D. Hartung, G. Koch, P.J. Klar, E. Mueller, S. Schlecht, Structural and Thermoelectric Properties of Nanostructured Nominally Stoichiometric $Pb_{1-x}Bi_xTe$ Prepared by Mechanical Alloying, J. Electron. Mater., 46 (2017) 5781-5791. https://doi.org/10.1007/s11664-017-5607-5.
[43] C.-H. Su, Design, growth and characterization of PbTe-based thermoelectric materials, Prog. Cryst. Growth Charact. Mater., 65 (2019) 47-94. https://doi.org/10.1016/j.pcrysgrow.2019.04.001.
[44] J.C. Wurst, J.A. Nelson, Lineal Intercept Technique for Measuring Grain Size in Two-Phase Polycrystalline Ceramics, J. Am. Ceram. Soc., 55 (1972) 109-109. https://doi.org/10.1111/j.1151-2916.1972.tb11224.x.
[45] M. Fusa, N. Yamamoto, K. Hasezaki, Measurement of Seebeck Coefficient and Conductive Behaviors of $Bi_2Te_{3-x}Se_x$(x=0.15-0.6) Thermoelectric Semiconductors without Harmful Dopants, Mater. Trans., 55 (2014) 942-946. https://doi.org/10.2320/matertrans.MB201301.

[46] K. Uemura, I. Nishida, Thermoelectric semiconductors and their applications, Nikkan-Kogyo, Tokyo, 1988, pp. 195-197.
[47] R.F. Bis, Temperature-pressure projection of lead telluride phase diagram, J. Phys. Chem. Solids, 24 (1963) 579-581. https://doi.org/10.1016/0022-3697(63)90155-0.
[48] J. Lin, K. Hsleh, R. Sharma, Y. Chang, The Pb-Te (lead-tellurium) system, Bull. Alloy Phase Diagr., 10 (1989) 340-347. https://doi.org/10.1007/BF02877589.

Supplementary data A.

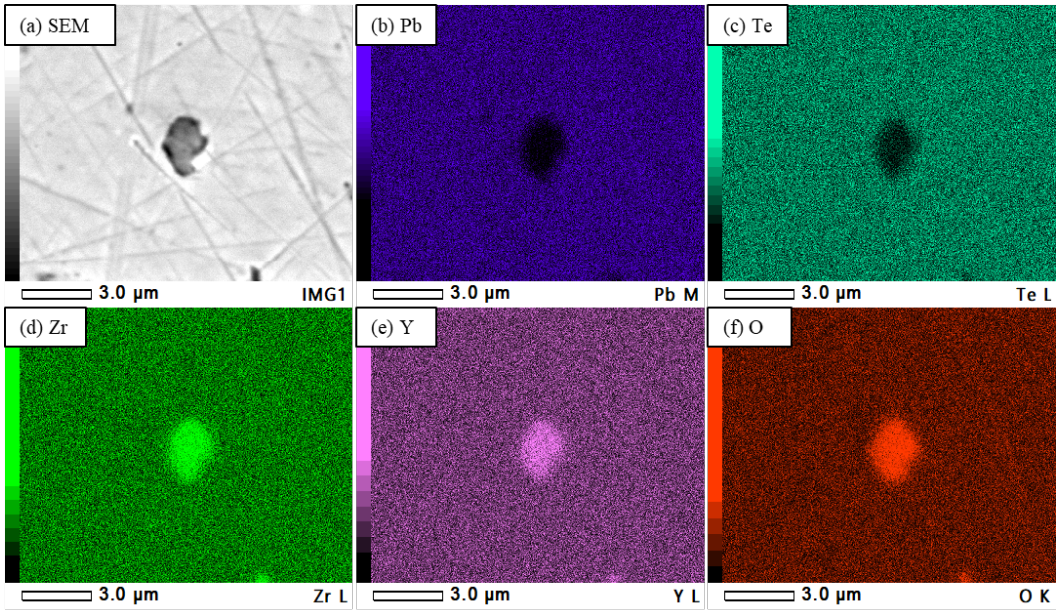

Supplementary fig. A EDS-derived elemental distribution of a PbTe sample milled at 2.5 Hz prepared by MG-HP. (a) SEM image, (b) Pb, (c) Te, (d) Zr, (e) Y and (f) O.

Supplementary fig. A(a) shows an SEM image of the MG-HP sample milled at 2.5 Hz. Except for dark particle, the matrix is dense, without pores or voids, confirming the observed relative densities. **Supplementary fig. A (b)–(f)** show the elemental distributions of Pb, Te, Zr, Y, and O determined by EDS, respectively. The matrix exhibits a uniform elemental distribution except for the presence of some particles with a diameter of around 2 µm resulting from the erosion of the YSZ vessel and balls. The MA-HP sample milled at 2.5 Hz exhibits similar features, i.e., uniform elemental distribution and presence of some YSZ particles. Contamination from milling vessels and balls increases when increased rotation speed, however, it does not affect the electrical properties.

Supplementary data B.

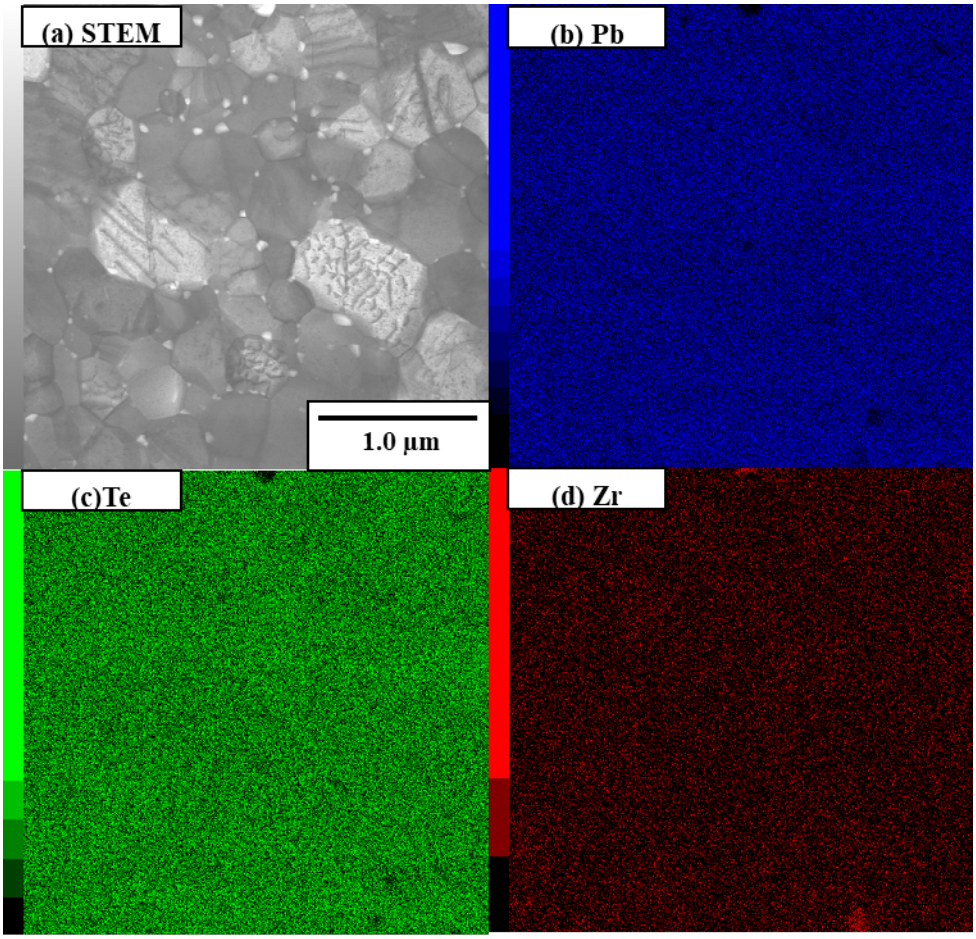

Supplementary fig. B (a) STEM micrographs of PbTe samples milled at 2.5 Hz prepared by MG-HP and the elemental distributions of (b) Pb, (c) Te, and (d) Zr determined by EDS.

Supplementary fig. B (a) shows the STEM micrograph of the sintered disk PbTe sample milled at 2.5 Hz prepared by MG-HP were investigated by transmission electron microscopy (TEM; JEOL, JEM-2100F). The grain size was approximately 0.5 µm, which corresponds to the observation by FIB-SEM in Fig. 2. The grains consisted of subgrain with approximately 50 nm in size.

Supplementary fig. B (b)−(d) show the elemental distributions of Pb, Te, and Zr. Each element was distributed homogeneously, and the second phase was not observed.

Supplementary data C.

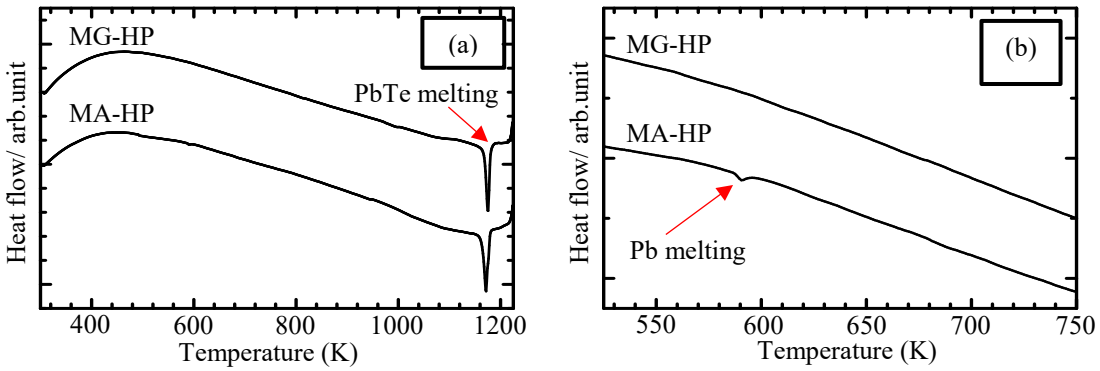

Supplementary fig. C DTA curves for PbTe MG-HP and MA-HP milled at 3.0 Hz. a) 300–1200 K, b) 500–750 K.

Supplementary fig. C (a) shows differential thermal analysis DTA curves for the PbTe endothermic reaction at the melting point and confirming Pb appears for MA-HP processed at 3.0 Hz by **Supplementary fig. C (b)**.